Ripple-like instability in the simulated gel phase of finite size phosphocholine bilayers

Vivien Walter [a],[*], Céline Ruscher [b], Adrien Gola [b], Carlos M. Marques [b], Olivier Benzerara [b], Fabrice Thalmann [b],[*]

[a] *Department of Chemistry, King's College London, Britannia House, 7 Trinity Street, SE1 1DB, London, United Kingdom*
[b] *Institut Charles Sadron, CNRS and University of Strasbourg, 23 rue du Loess, F-67034 Strasbourg Cedex 2, France*

ARTICLE INFO

ABSTRACT

Atomistic molecular dynamics simulations have reached a degree of maturity that makes it possible to investigate the lipid polymorphism of model bilayers over a wide range of temperatures. However if both the fluid L_α and tilted gel $L_{\beta'}$ states are routinely obtained, the $P_{\beta'}$ ripple phase of phosphatidylcholine lipid bilayers is still unsatifactorily described. Performing simulations of lipid bilayers made of different numbers of DPPC (1,2-dipalmitoylphosphatidylcholine) molecules ranging from 32 to 512, we demonstrate that the tilted gel phase $L_{\beta'}$ expected below the pretransition cannot be obtained for large systems (equal or larger than 94 DPPC molecules) through common simulations settings or temperature treatments. Large systems are instead found in a disordered gel phase which display configurations, topography and energies reminiscent from the ripple phase $P_{\beta'}$ observed between the pretransition and the main melting transition. We show how the state of the bilayers below the melting transition can be controlled and depends on thermal history and conditions of preparations. A mechanism for the observed topographic instability is suggested.

1. Introduction

Lipid membranes are fundamental components of living organisms, for their pivotal role in the structure and the biochemistry of the cells. Their properties are for a major part the consequence of the organization of the phospholipid molecules that compose them to a large extent. This organization is best revealed by experimenting with artificial lipid bilayers [1,2]. Through a perfect control of the molecular composition, an extended range of geometries and the possibility to insert membrane proteins and all sort of molecules, artificial bilayers have become a standard tool in modern biophysics [3,4].

A remarkable property of pure phospholipids bilayers is to exhibit a number of thermodynamic transitions upon temperature changes, meaning that they can be found in several phases including a crystalline phase L_c, a dense structured $L_{\beta'}$ tilted gel phase or a disordered fluid phase L_α upon increasing temperatures [3–6]. Decades ago, a new phase have been identified in the most common sort of phospholipid, the phosphocholines (PC lipids) [4,7–14]. This new phase, specific to the PC lipids and called the ripple phase $P_{\beta'}$, is characterized by important corrugation along the bilayer and the alternation between interdigitated or disordered lipids and more regularly packed ones. In pure lipid–water systems, the sequence of structures is accompanied by a sequence of phase transitions with calorimetric signature,

while X-ray diffraction makes it possible to recognize unambiguously the corresponding structures. For saturated identical acyl chains of lengths comprised between 14 and 20 carbons, these are by increasing temperature order: 1) the subtransition between L_c and $L_{\beta'}$, 2) the pretransition between $L_{\beta'}$ and $P_{\beta'}$ and 3) the main transition between $P_{\beta'}$ and L_α. The ripple phase is experimentally stable in pure bilayers of 1,2-dipalmitoylphosphatidylcholine (DMPC) between 16 and 24 °C, 1,2-dipalmitoylphosphatidylcholine (DPPC) between 34 and 41 °C and 1,2-distearoylphosphatidylcholine (DSPC) between 51 and 55 °C [3, 15].

This structure is sometimes presented as resulting from an alternation of gel and fluid lipid configurations [16–18]. There is no consensus regarding the cause [16,17,19–27] and the experimental structure is still subject to detailed investigations [28]. Ripple-like instability seems to be also a generic feature of various different numerical lipid models [29–32].

In a recent paper, Khakbaz and Klauda investigated the phase transition of DMPC and DPPC [33]. They reported formation of a structure resembling the $P_{\beta'}$ phase for DMPC bilayers in a range of temperature, while for DPPC only a transition from the tilted to the fluid phase was observed in bilayers composed of 70 lipids. More

---

recently, we investigated the phase transition of DPPC bilayers using Machine Learning algorithms [34]. In membranes composed of 212 lipids, we observed a transition at 315 K from a fluid phase to a condensed disordered phase presenting strong similarity to the ripple phase, but that persists well below the pretransition temperature of 307 K and the $L_{\beta'}$ gel tilted phase was never obtained directly from a quench of the L_{α} state.

In this article, we provide a detailed analysis of the nature of the phase of DPPC simulated with the CHARMM36 force field below its melting temperature. We investigate the state of DPPC bilayers at 288 K, for different system sizes and different thermal routes. While the $L_{\beta'}$ phase is observed for small systems, we found that a disordered phase, reminiscent of the $P_{\beta'}$ phase, occurs in larger systems. In particular, we noticed the formation of corrugations whose amplitude increases with the sizes of the systems investigated. We decide to call in this work this state the disordered gel phase L_{β}^d to differentiate it from both the tilted gel phase expected at these temperatures, and the true periodic ripple phase forming only at higher temperatures. By applying different thermal treatments, we characterize the metastability of DPPC and show that disordered gel is the preferred phase of simulated DPPC at 288 K, in the thermodynamic limit.

2. Material & methods

2.1. System description

DPPC bilayers were obtained using the CHARMM-GUI online Membrane Builder [35–38]. The size of the membrane was controlled *via* the number of lipids, ranging from 32 to 512 and with equal amounts of lipids in both leaflets. The bilayers were hydrated with water blocks of 10 nm on each side to prevent any interaction of the leaflets through the PBCs along the Z-axis. DPPE and DSPC bilayers made of 64 and 212 lipids were also prepared using the same process and characteristics. The exact composition of each system used is given in the Table A.1 of the Supplementary Materials. All initial coordinate files were made available on Zenodo [39].

The constructed systems were minimized in energy using a steepest descent algorithm and equilibrated by running two NVT simulations at 288 K for 10 ps, with respectively a 0.001 ps and a 0.002 ps step; and two NPT simulations at 288 K and 1 bar, with a 0.002 ps step for respectively 100 ps and 1 ns.

2.2. Simulation runs

Unless specified, the following conditions and parameters were used for all simulations. All simulations were performed using GROMACS 2016.4 [40,41] along with the CHARMM-36 all-atom force-field [42] (June 2015 version). The force field parameters for the lipid molecules were provided directly by CHARMM-GUI [43,44].

All the molecular dynamics simulations used the leap-frog integration algorithm [45] with a time step set to 2 fs. The temperature was controlled during the simulation using a Nosé–Hoover thermostat [46, 47] with a correlation time of $\tau_T = 0.4$ ps, and a Parrinello–Rahman semi-isotropic barostat [48,49] set to 1 bar in all directions was applied to the system (correlation time $\tau_P = 2.0$ ps, compressibility 4.5×10^{-5} bar^{-1}).

Lipid and water molecules were separately coupled to the thermostat. Following GROMACS recommendations for the CHARMM-36 all-atom force field, a Verlet cut-off scheme on grid cells was used with a distance of 1.2 nm, and non-bonded interactions cut-offs (Van der Waals and Coulombic) were also set to 1.2 nm. Fast smooth Particle-Mesh Ewald electrostatics was selected for handling the Coulombic interactions, with a grid spacing of 4 nm. A standard cut-off scheme with a force-switch smooth modifier at 1.0 nm was applied to the Van der Waals interactions. We did not account for long range energy and pressure corrections, and constrained all the hydrogen bonds of the system using the LINCS algorithm.

Molecular dynamics production runs lasted for a minimum of 50 ns. When temperature treatments occurred, the systems were simulated for another 50 ns to allow for the bilayer to reach equilibrium. The equilibrium was assessed by simulating DPPC bilayers made of 64 and 212 lipids at various temperatures ranging from 288 to 358 K and observing no difference in the system properties and characteristics between 25 and 450 ns of simulation, even at 288 K. The equilibrium assessments are provided in the Figures A.1 to A.4 of the Supplementary Materials. In all the other cases the analysis was performed on the last 25 ns of the simulations.

2.3. Analysis

The areas per lipid of the systems were measured using two different methods: (i) measure by projection of the bilayer onto the XY plane of the box, noted A_H^p, and (ii) measure by meshing of the water–lipid interfaces of each leaflet of the bilayer, written A_H^m. The projected area per lipid was measured directly in Gromacs by measuring the area of the simulation box in the XY plane and by dividing it by the number of lipids per leaflet. The meshed area per lipid was computed using Ovito 2.9. To do so, the surface of the water blocks at the water–lipid interface was meshed using a probe sphere radius of 6 and a smoothing level of 30 (arbitrary units specific to Ovito) after removing the lipid molecules. The area of the meshing was then divided by the total number of lipids in the bilayer.

The amplitude and the period of the corrugations were measured using the meshing of the water–lipid interface collected for the measurement of the area per lipid. The position of the vertices of the meshing were interpolated using SciPy [50] on a (200,200) uniform grid of the size of the simulation box, and the height of these 200×200 points were analyzed. This grid was directly used to generate the height maps. The amplitude of the corrugations, represented by the root mean square (RMS) height of the points on the grid, was calculated by subtracting the mean and then measuring the standard deviation of the height $\sigma(h)$. The period of the corrugations was calculated by computing the azimuthal power spectrum density (PSD) of the points of the grid and determining the frequency of the highest peak of the PSD.

To measure the local chain tilt direction, the positions of the atoms of the tails of the lipids were extracted from the simulation files using MDAnalysis [51,52]. The vectors from the first carbon atoms of each tail to all the carbon atoms of their respective tails were computed, before calculating the mean vector. The vector field was then created by binning the membrane in $n \times m$ squares and averaging over time the tilt direction vectors found in each square (X_i, Y_i). As a consequence, the vector field accounts for the average direction of the tails found at this location, but are not associated with given lipid molecules.

The enthalpy of the systems was extracted from the simulation using directly the tool provided with Gromacs, *gmx energy*. The systems used had strictly the exact same number of atoms, for both lipids and water molecules, to prevent changes due to the system composition. The (tilted) gel–fluid phase transition enthalpy was measured using the method from [53]. Briefly, the total enthalpy of a system simulated at different temperatures over a wide range, here 283 to 358 K, was collected. The effects of the temperature increase on the enthalpy, besides any phase transition, were removed from the measurement by subtracting the affine baseline measured in each phase. The values were then divided by the total number of lipids in the system, and the melting transition enthalpy was calculated by integrating the difference between the fitted gel and fluid baseline over the range of temperature at which the transition occurs (here 308 to 318 K, accounting for Gromacs accuracy in setting a temperature). For the tilted to disordered gel phase transition, the enthalpy was measured by bringing the two systems at the exact same temperature. The difference in enthalpy measured between these two systems was then divided by the total number of lipids in the system.
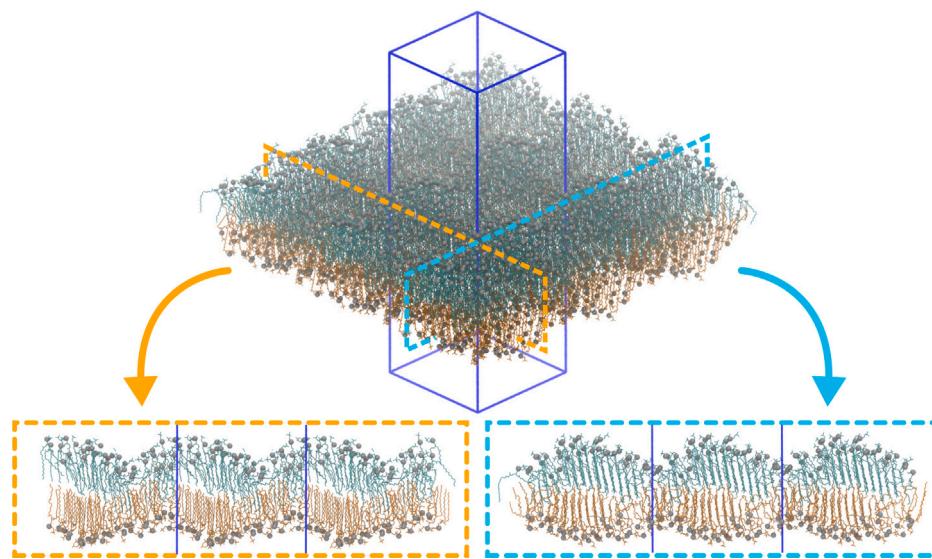
Fig. 1. DPPC bilayer made of 212 lipids simulated at 288 K right after construction and equilibration. 2.5 nm thick slices of the system along each axis are shown on the bottom, highlighting the corrugations of the membrane. Top and bottom lipid leaflets are colored respectively in cyan and orange while the phosphorus atoms are shown as silver beads. Hydrogen atoms were removed from the screenshot to improve readability. The PBC box is displayed using the blue plain lines.
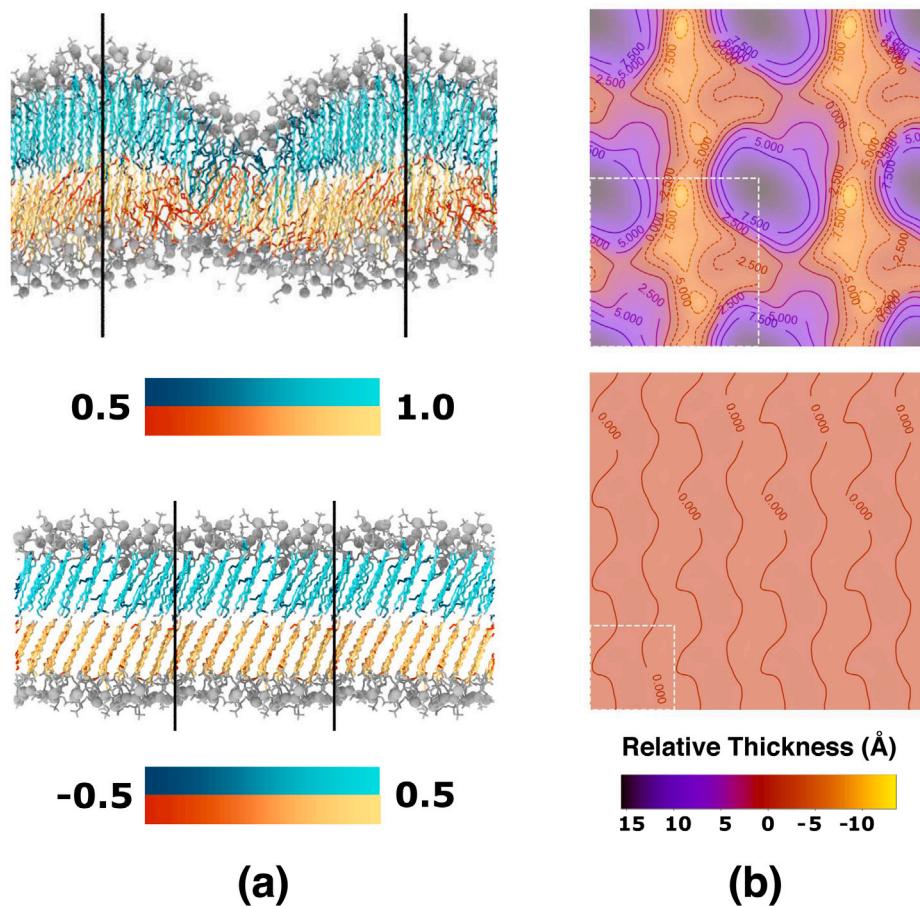

Fig. 2. (a) Representation of slices of the lipid membranes made of (Top) 256 and (Bottom) 64 lipid bilayers, with a color code on the tail atoms corresponding to their order parameters. (b) Topography of the upper leaflet of the membranes shown in (a), highlighting the corrugations observed in the membrane. Both contour plot shares the same color code and contour line scale, in Å. The white dashed line show the system before replication.
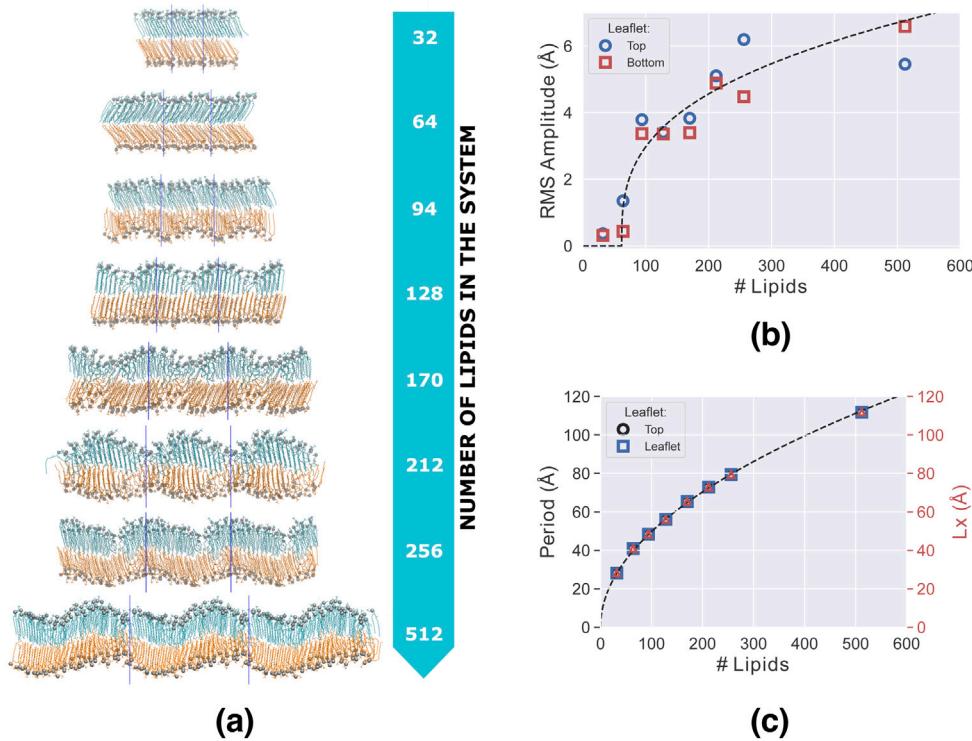
Fig. 3. Effect of the size of the simulation box on the geometry of bilayers. (a) 2.5 nm thick slices of the systems made with different amount of lipid molecules and simulated at 288 K. Measurement of the (b) amplitude, or h_{RMS} and (c) period of the corrugations observed in different systems versus the number of lipids. The evolution of the size of the box is shown on top of the period. Dashed lines are respectively the cubic root and square root fits of the data.

3. Results

3.1. Corrugation formation and characterization

We considered DPPC bilayers prepared with CHARMM-GUI at temperature $T = 288$ K with sizes ranging from 32 to 512 lipids. For small bilayers made of 64 lipids or less, we observed the formation of a smooth $L_{\beta'}$ tilted gel phase, in agreement with the numerous experiments and simulations reported in the literature [54]. The geometry of these bilayers remained stable over time, even after simulation runs up to 450 ns long. When larger systems (>94) lipids were concerned, we noticed the formation of a corrugation deforming significantly the leaftlets (cf Fig. 1).

The corrugations develop along both axis of the simulation box (X and Y). As already observed and investigated in details for DMPC by Khakbaz and Klauda [33], the molecular configurations of the lipids do not appear uniform along the corrugations, and the typical stretched tails of the gel phase seem to turn into the typical disordered tail configurations of the fluid phase in the thin portions of the corrugations where interdigitation happens. These variations in configuration can be highlighted by computing and mapping the local segment order parameter S_{mol} of each atom of each lipid (cf Fig. 2(a)).

We systematically characterized the corrugation and probed its evolution with system size. To quantify it in a more specific way, we investigated the topographic elevation function for each leaflet (see Fig. 2(b), topography for all membranes simulated in this study provided in Figures B.5 to B.8 of the Supplementary Materials.) from which we defined the amplitude of the corrugation as the root mean square (RMS) height h_{RMS} of the two water–lipid interfaces of the bilayers. The heights of the interfaces were obtained by meshing the water surface and removing the mean height of each leaflet. In these circumstances, h_{RMS} is equal to the standard deviation of the heights $\sigma(h)$. The leaflet corrugation amplitudes are identical for both leaflets even though cross section pictures might suggest otherwise (Fig. 3(a)). The corrugation

amplitude increases with system size but saturates for large systems (Fig. 3(b)). The longitudinal period of the corrugations always coincide with the periodic boundary conditions (PBC, see Fig. 3(c)). The power spectrum densities (PSD) used to measure the periods are given in the Figures B.9 and B.10 of the Supplementary Materials.

To better quantify the nature of the corrugation, we investigated the area per lipid using two methods: (i) *projection* in the (XY) plane of the box, i.e the area A_H^p of the box divided by the number of lipid; (ii) *meshing* of the water–lipid interface that enables the determination of the interfacial area A_H^m. Illustrations of the meshed area are shown in Figure B.11 of the Supplementary Materials. We found that the difference between interfacial and projected area per lipid

$$\alpha = \frac{A_H^m - A_H^p}{A_H^p} \tag{1}$$

provides an excellent characterization of the corrugated phase (Fig. 4). Indeed, α is three times larger for corrugated systems ($\alpha = 14 \pm 2\%$) than for tilted ones ($\alpha = 5 \pm 2\%$). All values of projected and meshed area, as well as area difference α, are given in the Table B.2 and in the Figure B.12 of the Supplementary Materials. The differentiation using usual methods such as the area per lipid or the tail order parameter achieved less significant results (cf Figures B.13 and B.14 of the Supplementary materials).

The local chain tilt direction in the XY plane was also determined and mapped. To account for lipid diffusion over time, instead of measuring and mapping the average orientation of each lipid, we decomposed the XY plane of the bilayer into a 16×16 grid and measured the orientation of the tails of the lipid found in each elements of the grid over time. This results in the vector fields shown in Fig. 5(a). As expected, tilts are uniform in the $L_{\beta'}$ state and present a random short-range correlation in the fluid L_α state. This was confirmed by the distribution of the angles with respect to the X-axis, as a function of the height on the leaflet. In the corrugated systems, the local chain tilts displays long-range variations. The angle distribution of the corrugated
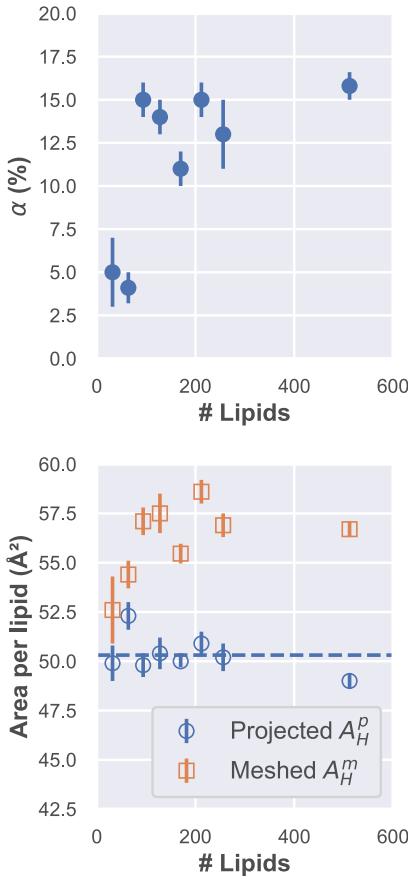
Fig. 4. (Top) Differences between the area per lipid measured by surface meshing and by projection in the XY plane α (in %) and (Bottom) evolution of each type of area per lipid for different system sizes. Blue dashed line on the bottom graph is the average projected area per lipid.

Fig. 5. (a) Average field of the DPPC tails orientation vector projected in the XY plane over a 16×16 cubic lattice of the bilayer (Top) in the disordered gel phase, (Middle) in the tilted gel phase and (Bottom) in the fluid phase. Only one leaflet of the membrane is shown for each system. (b) Respective scatter distribution of the angles between the tails of the lipids and the X-axis of the membrane, as a function of the height on the leaflet. The measurement were performed on both top and bottom leaflets, respectively colored in cyan and in orange.

systems shows that small heights have random orientation similar to the fluid.

We also probed the sensitivity of the corrugation to modifications of space group. A simple change from cubic to rectangular simulation boxes with $L_x = 2L_y$ shows commensurate corrugations periods. Moreover we carry out simulations in hexagonal and monoclinic simulation boxes counting 128 lipids. Both of these systems were found to be corrugated, with modulation vectors directed along the PBC/crystallographic directions (Fig. 6).

To release residual stress on the bilayer configuration that could have been brought by the semi-isotropic barostat, an anisotropic barostat was applied to the systems, with 1 bar and a 4.5×10^{-5} bar^{-1} compressibility set along each axes, and the pressure crossed terms set to 0 for both pressure and compressibility. We found that releasing residual anisotropic stress did not modify the structure of the bilayers. After this simulation run, the system was still found in a corrugated state, as shown in Fig. 7, with a relative area increase α of $11.9 \pm 0.8\%$ and a RMS corrugation amplitude of 4.89 Å comparable to the amplitude before the run (5.18 Å). We therefore conclude from this result that both tilted gel and corrugated states behave as a cohesive, solid state on the simulated time scales. They also display significant residual static stresses of 0.8 and 1.0 bars respectively in the X and the Y directions. Based on these characterizations we refer to the corrugated state as the *disordered* gel state, noted here L_β^d, to make a clear distinction between these configurations and those of the 1D modulated ripple phase $P_{\beta'}$ that has only been experimentally reported above the pretransition temperature, and of the tilted gel phase $L_{\beta'}$ which usually forms at these temperatures.
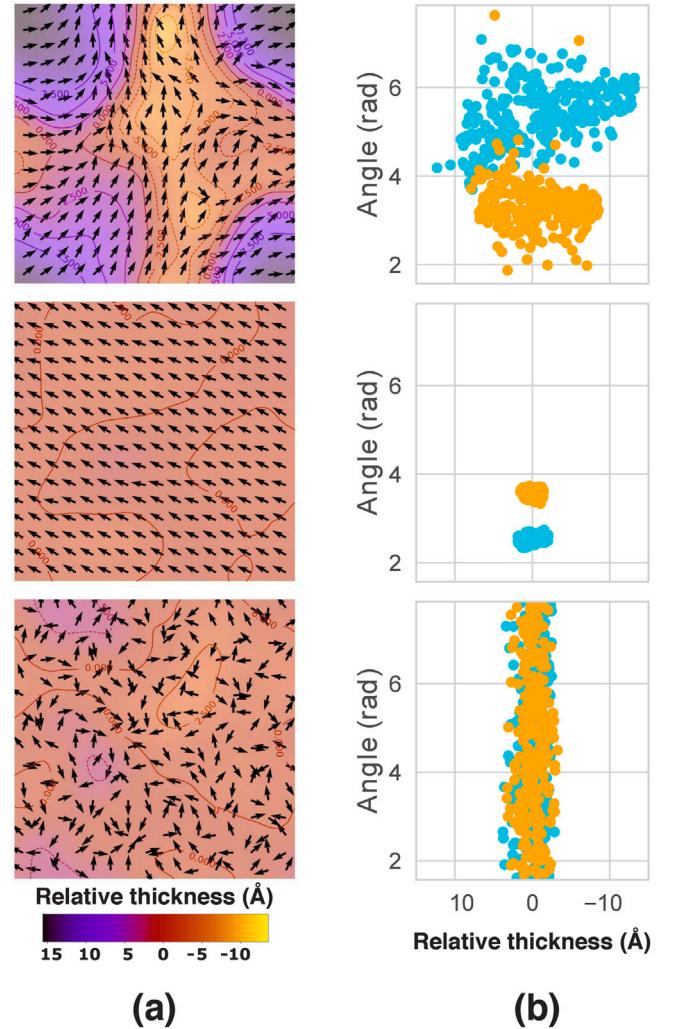
Finally one can wonder whether the appearance of the corrugation is restricted to DPPC or DMPC. To answer this question, we probed the effect of the tail and the head groups by considering the longer-tailed DSPC and the ethanolamine-based DPPE. As shown in Fig. 8, the large DSPC systems were found in the disordered gel state while the DPPE systems remained in the expected homogeneous tilted gel state. The respective area differences of these systems are 12 ± 1 and $5 \pm 1\%$.

The average chain tilt angle in the DPPC $L_{\beta'}$ state was found to be peaked around an average value of 38°, larger than the accepted experimental value (31°). The chain packing in the $L_{\beta'}$ state was also investigated on a single configuration frame, by projecting the carbon chain positions onto a plane orthogonal to the average carbon chain direction. The average chain positions appear to occupy the nodes of an hexagonal lattice, with an area per chain of the order of 20 Å^2 (Fig. E22, Supplementary Materials). The crystalline order is not perfect, with the presence of dislocations and a significant chain mobility during the simulation. The defects, chain mobility and thermal fluctuations did not allow us to make a closer comparison with existing crystallographic data. Altogether, it seems that the numerical $L_{\beta'}$ phase is in qualitative
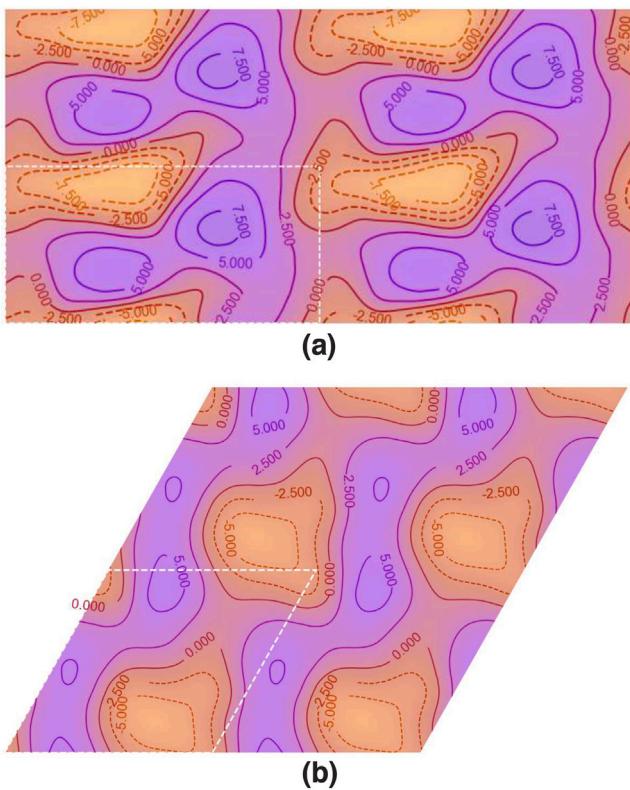
Fig. 6. Topography of bilayers (a) made of 188 DPPC molecules in a simulation box with $L_x = 2L_y$ and (b) made of 128 DPPC molecules in an hexagonal simulation box, both simulated at 288 K.
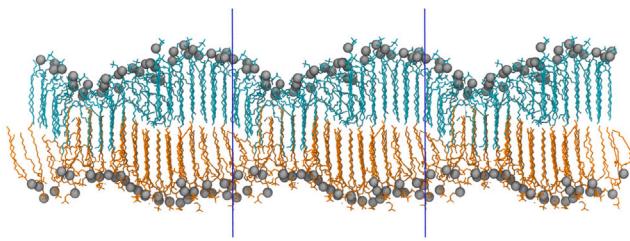

Fig. 7. Slice of the 212 DPPC molecule system obtained after being simulated at 288 K for 50 ns with an anisotropic barostat.

agreement with experimental findings, with a slightly too large tilt angle value.

3.2. Influence of thermal history

The previous observations suggest that disordered L_β^d and tilted $L_{\beta'}$ gel states are two competing states whose appearance seem to be correlated to the system size for freshly thermalized systems generated with CHARMM-GUI. In what follows we probe the sensitivity of the stability of these phases to different routes of thermal treatments.

We focus our analysis on two system sizes: 64 lipids, which has been found in the $L_{\beta'}$ phase, and 256 lipids which has been found in the L_β^d. Both systems were subjected to the following thermal treatment: starting from $T = 288$ K, systems were annealed at $T = 358$ K in the fluid phase. These systems are respectively named pc64-A and pc256-A, for annealing. They were then cooled down to $T = 288$ K in two different ways: either with a brutal fast cooling, named here quenched, or with a slow gradual cooling of 1 K/ns that we denote

gentle cooling. The quenched systems are noted pc64-AQ and pc256-AQ (annealing–quenching), and the cooled systems called pc64-AC and pc256-AC (annealing–cooling).

We first notice that whatever the thermal history, large systems were always found in the disordered gel state as shown in Fig. 9. Gentle cooling of small systems allowed them to recover the $L_{\beta'}$ phase while quenching lead to L_β^d phase. As in this latter case, either phases could be obtained depending on the thermal history, we conclude that the disordered gel is metastable with respect to the tilted gel for small systems. Furthermore, we can note that both the gently cooled and the quenched systems have a final projected area per lipid A_H^p (respectively 50.1 ± 0.7 and 50.8 ± 0.8 Å^2) close to the average projected area of 50 Å^2 found for systems of all sizes, starting from the value of 52.3 Å^2 before temperature treatment (cf Fig. 4).

As large systems of 256 lipids were never spontaneously found in the $L_{\beta'}$ state, we decided to force them into this state by duplicating along both X and Y directions the 64 $L_{\beta'}$ system. The flat tilted duplicated system was found to be stable on the simulation time scale, suggesting that $L_{\beta'}$ could be either stable or metastable in large systems too. The nature of the relevant stable thermodynamic phase for large systems remains an open question, while our simulations clearly favor the disordered gel state L_β^d. Measurements of the difference in area α can be found in the Figure B.12 of the Supplementary Materials. Additionally, measurement of the order parameter S_{mol} is given in the Figure C.18 of the Supplementary Materials.

3.3. Thermodynamics of tilted and disordered states

Since the small systems made of 64 lipids can be prepared and controlled to reach all the observed phases, we used them to compare the energetic properties of the respective gel state. Having in mind the idea of a complex underlying potential energy landscape composed of several minima located at different energy levels, we probe how far the disordered gel phase stands energetically from the tilted gel phase minimum. Therefore we performed an energy minimization using conjugate gradient to remove thermal fluctuations on the tilted and disordered gel configurations. We found $\Delta E_P = E_P(\text{disordered}) - E_P(\text{tilted}) = 64$ kJ/mol, meaning that if both states are metastable, the tilted system is the most stable one. In addition, we also computed the difference in enthalpy between the disordered and the tilted thermalized gel phases. To this aim, we used the same initial states, after quenching or gentle cooling but without energy minimization. Since the two systems share the same atomic compositions (same number of lipid, water molecules and constraints), the difference in enthalpy (kinetic and potential energy according to the force field, plus the PV contribution) at a given temperature should be characteristic of the enthalpy difference between the two states. We found an enthalpy difference of 12 ± 4 kJ/mol at 288 K. Snapshots of the systems and measurement are shown in Figure D.19 and D.20 of the Supplementary Materials. This value is higher than the one reported experimentally for the calorimetric gel to ripple phase pretransition, 4.6 kJ/mol [4] but obtained at a higher temperature. We therefore repeated the measure after rising both systems at a temperature close to the pretransition temperature, namely 305 K, and then found a difference in enthalpy of 3.9 ± 0.4 kJ/mol now compatible with experimental measurements. It is essential to note here that, in order to obtain a disordered system configuration at 305 K, the system had first to be annealed at 375 K instead of 358 K, meaning that the difference in temperature required for quenching should be at least of 70 K in order to obtain the L_β^d phase (see Figure D.21 of the Supplementary Materials).

The enthalpy of the $L_\beta^d \longrightarrow L_\alpha$ transition was also measured in our small systems. This was performed by simulating the 64 DPPC system at temperatures ranging from 283 to 358 K and by removing the change in enthalpy due to the change in temperature (data shown in Figure D.22 Supplementary Materials). The transition enthalpy was found equal to 27.3 kJ/mol, which is also comparable with the experimental
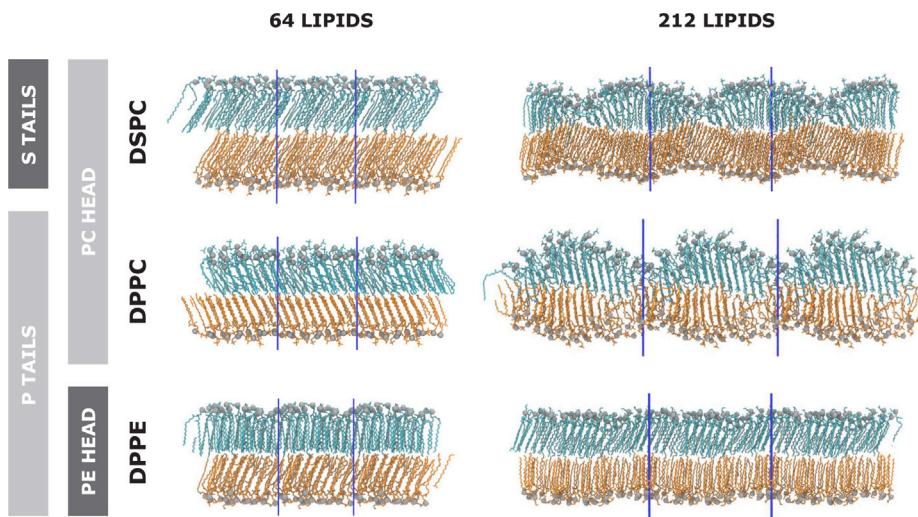
64 LIPIDS   **212 LIPIDS**

Fig. 8. Profiles of bilayers made of 64 or 212 lipids, either with DPPC, DSPC or DPPE, after a 50 ns simulation at 288 K. Only the DPPE membrane remained in the tilted gel phase when constructed with a large number of lipids.
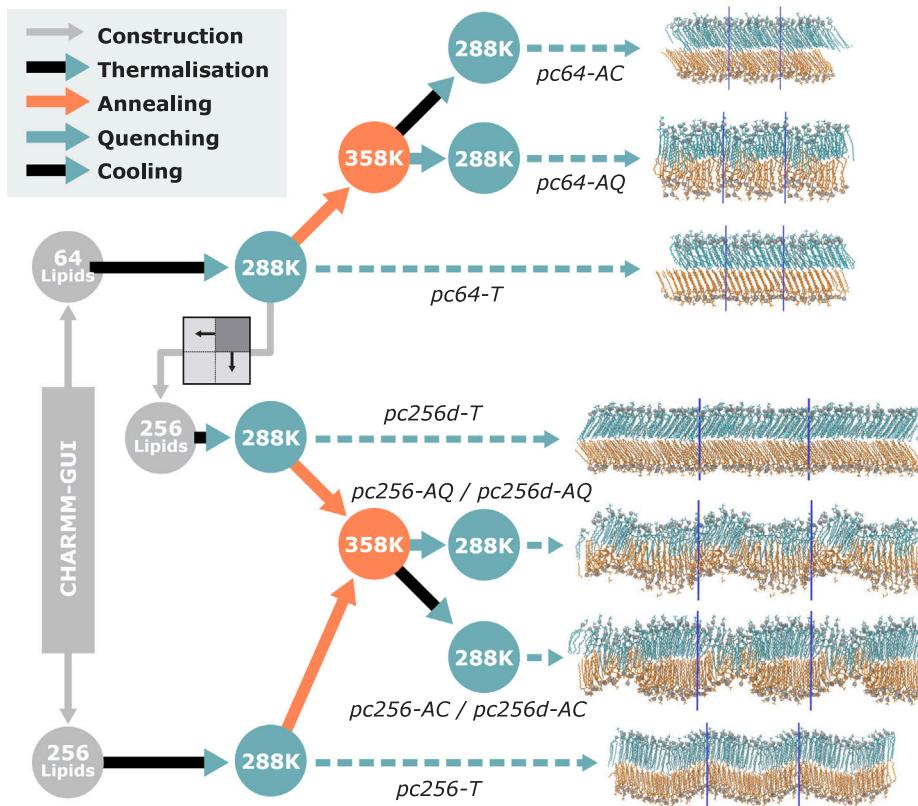

Fig. 9. Synopsis of the different thermal trajectories, showing the systems obtained for different cooling rates as well as the systems they originated from. Only the results from the 256 DPPC system obtained by replication of the 64 lipid system are shown for the quenching and cooling experiments. Results for the 256 DPPC system constructed by CHARMM-GUI, as well as the intermediate systems, are shown in the Figure C.15 to C.17 of the Supplementary Materials.

reported values *circa* 32.2 kJ/mol [4]. We can conclude that despite the approximations, and the absence of quantum corrections to the bond vibrations contributions, the CHARMM36 force field thermodynamic predictions seem in good agreement with experimental observations.

4. Discussion

A careful inspection of the corrugations shows that the topographic modulation is imposed by the periodicity of the simulation box. The corrugation shows finite system size dependence, as its amplitude increases up to sizes of the order of $L_x = 8$ nm where the modulation saturates to a value of 7 ± 1 Å. Assuming a sine-like corrugation, this maximum RMS amplitude measured can be converted into a peak-to-peak amplitude of 2.0 ± 0.2 nm similar to the previously published values of 2.4 nm for the DPPC or even 1.8 nm in DMPC bilayers [28, 55]. The saturation of the corrugation amplitude is expected, given that it can only reach a fraction of the total membrane thickness. The

associated lateral length 8 nm can therefore be considered as a lower bound of the instability characteristic longitudinal length scale.

We believe that the relative difference between the interfacial area and the projected one, α, introduced in Eq. (1) can be taken as a relevant order parameter for the transition between the $L_{\beta'}$ and the disordered gel phases L_{β}^{d}. The latter being reminiscent of the $P_{\beta'}$ ripple phase, α could be seen as a critical parameter to investigate the existence of the ripple phase and discriminate it from the tilted gel or from the fluid phase.

However, unlike experiments, the numerical instability occurs along two orthogonal directions, or along the hexagonal axes. Non-square boxes fail to select only one modulation direction. We nevertheless think that the numerical corrugation instability is related to the experimental ripple instability, as also suggested by the dependence of the presence of corrugation to the chemical nature of the heads and tails of the lipids. Indeed, experiments have shown that the ripple phase is specific for the phosphocholine (PC) lipids [54,56].

Another striking observation is the insensitivity of large systems (256 lipids) to thermal treatment which leads systematically to a disordered gel state. On the opposite, small systems can alternate between both phases. However, when thermalized at low temperatures from CHARMM-GUI or slowly quenched, they end up preferentially into the tilted gel state, suggesting that in the range of temperatures investigated the $L_{\beta'}$ state is thermodynamically favored. By contrast the $L_{\beta'}$ state is never selected spontaneously by larger systems. For the latter, MD suggests that the disordered gel state L_{β}^{d} is the most preferred state for all temperatures below melting. Metastability and kinetic effects are certainly significant and may hide to true nature of the stable phase.

Assuming that the difference between tilted and disordered gels has something to do with the pretransition, we found an enthalpy difference 3 times larger than the premelting latent heat at 288 K, and of the same order of magnitude at 305 K, close to the observed experimental transition. This points towards the relevance of disordered gel state L_{β}^{d} as a ripple state analogue. Moreover the higher enthalpy of the disordered gel with respect to the tilted gel is consistent with a $L_{\beta'} \longrightarrow L_{\beta}^{d} \longrightarrow L_{\alpha}$ sequence of transitions as temperature is increased.

A recurrent question arises as to estimating the importance of molecular chirality in the ripple phase formation. It was for instance argued that racemic mixtures of L- and D-DPPC molecules do not exhibit the $L_{c} \rightarrow L_{\beta'}$ subtransition [57]. However, as far as the pretransition is concerned, while changing fraction of stereoisomeres may change the pretransition temperature, it has been demonstrated experimentally that the lipid chirality was not having much effect on the ripple structure of the membrane. [12,58,59]. In our case, the initial membrane configurations were generated using the CHARMM-GUI interface, and all the lipids were (for instance) L-DPPC (R) or equivalently *sn*3-glycero stereoisomers [3,60]. We defined and measured a chiral parameter defined as the average normalized determinant of the vector joining the central glycerol carbon and the geometrical middle point of the two terminal methyl groups, the vector joining the central glycerol carbon and the nitrogen headgroup atom and the simulation box normal vector $\vec{e}_{z}$ (Fig. E.25, Supplementary Materials). The normalization was such that the parameter amounts to measuring the average sine angle between the headgroup and tailgroup projected vectors onto the XY plane. Only in the tilted $L_{\beta'}$ state was the parameter found to take a significant value of about -0.10. In both the fluid and disorder gel state, this parameter was found positive and close to $+1.0 - 2.0 \times 10^{-2}$. Upon this criterion, the ripple-like state is less chiral than the tilted gel state. At a larger scale, the instability could be associated with a macroscopic chirality, as suggested by [24,61]. We understand that the Helfrich and Prost elastic term underlying this chiral mechanism would couple a director vector linked to each lipid molecule with the principal directions of curvatures of the local meshed surface, with a preferential orientation of 45 or 135° of the director with respect to these principal directions. There should therefore be, for instance, some winding of the average chain orientation along the rim of the shallow region in
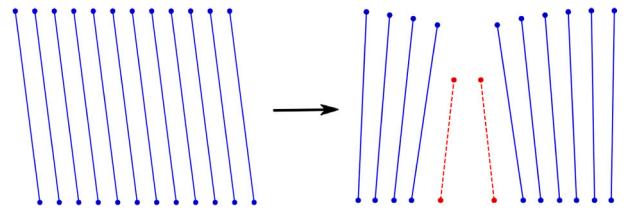

Fig. 10. Schematic representation of the mechanical instability occurring in a simple one dimensional lipid chain model, where the tilted state has a higher energy than a locally disordered state. The gain in energy originates mostly from the hydration term. Blue solid rods stand for gel state, red dashed rods for fluid state.

Fig. 5, which does not look obvious. Our conclusion is therefore that chirality in unlikely to play a large role in the numerical instability that we observe.

The reason of the outcome of a ripple instability below the melting temperature has to be explained. Our simulations point out to a competition between an homogeneous tilted state and an inhomogeneous corrugated state. The transition between these states is discontinuous. The corrugated state is not very tilted, and partially melted, or disordered, or interdigitated. We suggest now a possible mechanism explaining the observed situation. The tilted phase can be understood as the result of a frustration between lipid headgroups which try to increase their exposure to water in the interface region, lipid chains which try to reach an optimal packing density as a result of cohesive forces, and chain stiffness for which the introduction of *gauche* dihedral angles is unfavorable at low temperatures. Tilt allows lipids to optimize simultaneously those three constraints. On the other hand, melting a lipid chain enables the release of the constraint acting on the chain stiffness, and makes it possible to increase the hydration free-energy by reducing the membrane thickness. Below melting temperature, thermodynamics makes it unfavorable to melt all the lipid molecules. However, some local disordering of the lipids may still be favorable, increasing the hydration of the headgroups without need of spending too much energy in melting the chains.

Based upon those considerations, we designed a simple one dimensional lipid chain model that supports the idea that in a temperature range just below melting, the homogeneous tilted state is energetically unstable with respect to a local corrugation of the bilayer, see Fig. 10. Details of the parameterization of the model and further results are presented in the Appendix F of the Supplementary Materials. The novel optimal state is much less tilted than the all-gel state, in agreement with Fig. E.23, but the fraction of melted chains remains small. Such an alternation of melted and gel chains can be traced back to the models of Falkowitz et al. [17], Marder et al. [19] or more recently Heimburg [18]. The importance of hydration and tilt was also emphasized by Carlson and Sethna [21]. Our approach combines all the elements – hydration, tilt, local melting – that seem important in producing the observed thickness modulation. More work is needed to establish whether such approach can successfully predict an asymmetric, 1D modulated ripple phase. We conclude that the thickness modulation might indeed be caused by a subtle interplay between headgroup hydration, hydrophobic chain packing, *trans-gauche* isomerization and tilt elasticity energy terms.

5. Conclusion

We have successfully demonstrated in this work how the size of the simulation box influences the ripple-like instability in a PC membrane simulated with the Charmm36 force field at low temperature, where it is usually expected to be in the tilted gel $L_{\beta'}$ phase. This unexpected organization, which we called the disordered gel phase L_{β}^{d}, does not appear in small systems, which is consistent with the results from Khakbaz and Klauda [33] as well as with our results [34]. The energy

and geometry analyses demonstrated that this disordered gel phase has much in common with the $P_{\beta'}$ phase. Furthermore, this instability was not observed with PE lipids, in agreement with experimental findings. For small systems, we found ways of preparing the system in either tilted gel or disordered gel states by acting on the thermal treatment. More work is needed to determine whether the Charmm36 force-field can describe a one-dimensional $P_{\beta'}$ spatial thickness modulation, with the right periodicity, and at which temperatures. Our work suggests that simulations will have to be guided to the desired structure. Finally, we conclude that the ripple instability appears as a generic mechanism adopted by the phosphatidylcholine lipids to increase the headgroup hydration while still satisfying the packing constraints, at the expense of a mild cost in disordering/melting a small fraction of the chains.

Declaration of competing interest

The authors declare that they have no known competing financial interests or personal relationships that could have appeared to influence the work reported in this paper.

Acknowledgments

Appendix A. Supplementary data

Supplementary material related to this article can be found online at https://doi.org/10.1016/j.bbamem.2021.183714.

References

[1] O.G. Mouritsen, Life-as a Matter of Fat: The Emerging Science of Lipidomics, Springer, 2005.

[2] R. Dimova, C.M. Marques (Eds.), The giant vesicle book, first ed., CRC Press, Taylor and Francis, 2019.

[3] D. Marsh, Handbook of Lipid Bilayers, second ed., CRC Press, Boca Raton, 2013.

[4] G. Cevc, D. Marsh, Phospholipid Bilayers. Physical Principles and Models, John Wiley & Sons, New-York, 1987.

[5] J. Seddon, R. Templer, Polymorphism of lipid-water systems, in: Handbook of Biological Physics, Elsevier, 1995, pp. 97–160, http://dx.doi.org/10.1016/s1383-8121(06)80020-5.

[6] T. Heimburg, Thermal Biophysics of Membranes, Wiley-VCH, 2007.

[7] A. Tardieu, V. Luzzati, F.C. Reman, Structure and polymorphism of the hydrocarbon chains of lipids: A study of lecithin-water phases, J. Mol. Biol. 75 (4) (1973) 719–733.

[8] M.J. Janiak, D.M. Small, G.G. Shipley, Nature of the thermal pretransition of synthetic phospholipids: dimyristoyl- and dipalmitoyllecithin, Biochemistry 15 (21) (1976) 4575–4580, http://dx.doi.org/10.1021/bi00666a005.

[9] E.J. Luna, H.M. McConnell, The intermediate monoclinic phase of phosphatidyl-cholines, Biomembranes 466 (3) (1977) 381–392, http://dx.doi.org/10.1016/0005-2736(77)90331-5.

[10] M.J. Ruocco, G. Shipley, Characterization of the sub-transition of hydrated dipalmitoylphosphatidylcholine bilayers. Kinetic, hydration and structural study, Biomembranes 691 (2) (1982) 309–320, http://dx.doi.org/10.1016/0005-2736(82)90420-5.

[11] M.J. Ruocco, G.G. Shipley, Characterization of the sub-transition of hydrated dipalmitoylphosphatidylcholine bilayers, Biomembranes 684 (1) (1982) 59–66, http://dx.doi.org/10.1016/0005-2736(82)90049-9.

[12] J. Katsaras, V.A. Raghunathan, Molecular chirality and the "ripple" phase of phosphatidylcholine multibilayers, Phys. Rev. Lett. 74 (11) (1995) 2022–2025.

[13] W.J. Sun, S. Tristram-Nagle, R.M. Suter, J.F. Nagle, Structure of the ripple phase in lecithin bilayers, Proc. Natl. Acad. Sci. 93 (14) (1996) 7008–7012, http://dx.doi.org/10.1073/pnas.93.14.7008.

[14] C. Leidy, T. Kaasgaard, J.H. Crowe, O.G. Mouritsen, K.J. rgensen, Ripples and the formation of anisotropic lipid domains: Imaging two-component supported double bilayers by atomic force microscopy, Biophys. J. 83 (5) (2002) 2625–2633, http://dx.doi.org/10.1016/s0006-3495(02)75273-9.

[15] R.N.A.H. Lewis, N. Mak, R.N. McElhaney, A differential scanning calorimetric study of the thermotropic phase behavior of model membranes composed of phosphatidylcholines containing linear saturated fatty acyl chains, Biochemistry 26 (19) (1987) 6118–6126, http://dx.doi.org/10.1021/bi00393a026.

[16] S. Doniach, A thermodynamic model for the monoclinic (ripple) phase of hydrated phospholipid bilayers, J. Chem. Phys. 70 (10) (1979) 4587–4596, http://dx.doi.org/10.1063/1.437292.

[17] M.S. Falkovitz, M. Seul, H.L. Frisch, H.M. McConnell, Theory of periodic structures in lipid bilayer membranes, Proc. Natl. Acad. Sci. 79 (12) (1982) 3918–3921, http://dx.doi.org/10.1073/pnas.79.12.3918.

[18] T. Heimburg, A model for the lipid pretransition: coupling of ripple formation with the chain-melting transition, Biophys. J. 78 (2000) 1154–1165.

[19] M. Marder, H.L. Frisch, J.S. Langer, H.M. McConnell, Theory of the intermediate rippled phase of phospholipid bilayers, Proc. Natl. Acad. Sci. 81 (20) (1984) 6559–6561, http://dx.doi.org/10.1073/pnas.81.20.6559.

[20] M.H. Hawton, W.J. Keeler, Van der Waals energy of lecithins in the ripple phase, Phys. Rev. A 33 (1986) 3333–3340, http://dx.doi.org/10.1103/PhysRevA.33.3333.

[21] J.M. Carlson, J.P. Sethna, Theory of the ripple phase in hydrated phospholipid bilayers, Phys. Rev. A 36 (7) (1987) 3359–3374, http://dx.doi.org/10.1103/physreva.36.3359.

[22] L. Smeller, S. Györgyi, A statistical mechanical model of the pre- and sub-transitions of lecithin membranes, J. Theoret. Biol. 137 (2) (1989) 203–214, http://dx.doi.org/10.1016/s0022-5193(89)80206-1.

[23] K. Honda, H. Kimura, Theory on formation of the ripple phase in bilayer membranes, J. Phys. Soc. Japan 60 (4) (1991) 1212–1215, http://dx.doi.org/10.1143/jpsj.60.1212.

[24] T.C. Lubensky, F.C. MacKintosh, Theory of "ripple" phases of lipid bilayers, Phys. Rev. Lett. 71 (10) (1993) 1565–1568, http://dx.doi.org/10.1103/physrevlett.71.1565.

[25] J.-B. Fournier, Coupling between membrane tilt-difference and dilation: A new "ripple" instability and multiple crystalline inclusions phases, Europhys. Lett. 43 (6) (1998) 725–730, http://dx.doi.org/10.1209/epl/i1998-00424-4.

[26] C. Misbah, J. Duplat, B. Houchmandzadeh, Transition to ripple phases in hydrated amphiphiles, Phys. Rev. Lett. 80 (20) (1998) 4598–4601, http://dx.doi.org/10.1103/physrevlett.80.4598.

[27] K. Sengupta, V.A. Raghunathan, Y. Hatwalne, Role of tilt order in the asymmetric ripple phase of phospholipid bilayers, Phys. Rev. Lett. 87 (5) (2001) http://dx.doi.org/10.1103/physrevlett.87.055705.

[28] K. Akabori, J.F. Nagle, Structure of the DMPC lipid bilayer ripple phase, Soft Matter 11 (2015) 918–926.

[29] A.H. de Vries, S. Yefimov, A.E. Mark, S.J. Marrink, Molecular structure of the lecithin ripple phase, Proc. Natl. Acad. Sci. 102 (15) (2005) 5392–5396, http://dx.doi.org/10.1073/pnas.0408249102.

[30] O. Lenz, F. Schmid, Structure of symmetric and asymmetric "ripple" phases in lipid bilayers, Phys. Rev. Lett. 98 (058104) (2007).

[31] R. Chen, D. Poger, A.E. Mark, Effect of high pressure on fully hydrated DPPC and POPC bilayers, J. Phys. Chem. B 115 (5) (2011) 1038–1044, http://dx.doi.org/10.1021/jp110002q.

[32] A. Debnath, F.M. Thakkar, V. Kumaran, P.K. Maiti, K.G. Ayappa, Laterally structured ripple and square phases with one and two dimensional thickness modulations in a model bilayer system, Soft Matter 10 (2014) 7630–7637.

[33] P. Khakbaz, J.B. Klauda, Investigation of phase transitions of saturated phosphocholine lipid bilayers via molecular dynamics simulations, Biomembranes 1860 (8) (2018) 1489–1501.

[34] V. Walter, C. Ruscher, O. Benzerara, C.M. Marques, F. Thalmann, A machine learning study of the two states model for lipid bilayer phase transitions, Phys. Chem. Chem. Phys. 22 (34) (2020) 19147–19154, http://dx.doi.org/10.1039/d0cp02058c.

[35] S. Jo, T. Kim, W. Im, Automated builder and database of protein/membrane complexes for molecular dynamics simulations, PLoS ONE 2 (9) (2007) 880.

[36] S. Jo, T. Kim, V.G. Iyer, W. Im, CHARMM-GUI: A web-based graphical user interface for CHARMM, J. Comput. Chem. 29 (2008) 1859–1865.

[37] S. Jo, J.B. Lim, J.B. Klauda, W. Im, CHARMM-GUI Membrane builder for mixed bilayers and its application to yeast membranes, Biophys. J. 97 (2009) 50–58.

[38] E.L. Wu, X. Cheng, S. Jo, H. Rui, H.K. Song, E.M. Davila-Contreras, Y. Qi, J. Lee, V. Monje-Galvan, R.M. Venable, J.B. Klauda, W. Im, CHARMM-GUI Membrane builder toward realistic biological membrane simulations, J. Chem. Theory Comput. 35 (2014) 1997–2004.

[39] Zenodo repo, 2021, URL: http://dx.doi.org/10.5281/zenodo.4522359.

[40] H. Berendsen, D. van der Spoel, R. van Drunen, GROMACS: A message-passing parallel molecular dynamics implementation, Comput. Phys. Comm. (1995).

[41] M.J. Abraham, T. Murtola, R. Schulz, S. Páll, J.C. Smith, B. Hess, E. Lindahl, GROMACS: High performance molecular simulations through multi-level parallelism from laptops to supercomputers, SoftwareX (2015).

[42] R.B. Best, X. Zhu, J. Shim, P.E.M. Lopes, J. Mittal, M. Feig, A.D. MacKerell Jr., Optimization of the additive CHARMM all-atom protein force field targeting improved sampling of the backbone phi, psi and side-chain khi1 and khi2 dihedral angles, J. Chem. Theory Comput. 8 (9) (2012) 3257–3273.

[43] B.R. Brooks, C.L. Brooks III, A.D. MacKerell Jr, L. Nilsson, R.J. Petrella, B. Roux, Y. Won, G. Archontis, C. Bartels, S. Boresch, A. Caflisch, L. Caves, Q. Cui, A.R. Dinner, M. Feig, S. Fischer, J. Gao, M. Hodoscek, W. Im, K. Kuczera, T. Lazaridis, J. Ma, V. Ovchinnikov, E. Paci, R.W. Pastor, C.B. Post, J.Z. Pu, M. Schaefer, B. Tidor, R.M. Venable, H.L. Woodcock, X. Wu, W. Yang, D.M. York, M. Karplus, CHARMM: The biomolecular simulation program, J. Comput. Chem. 30 (2009) 1545–1614.

[44] J. Lee, X. Cheng, J.M. Swails, M.S. Yeom, P.K. Eastman, J.A. Lemkul, S. Wei, J. Buckner, J.C. Jeong, Y. Qi, S. Jo, V.S. Pande, D.A. Case, C.L. Brooks III, A.D. MacKerell Jr, J.B. Klauda, W. Im, CHARMM-GUI Input generator for NAMD, GROMACS, AMBER, OpenMM, and CHARMM/OpenMM simulations using the CHARMM36 additive force field, J. Chem. Theory Comput. 12 (1) (2016) 405–413.

[45] R.W. Hockney, S.P. Goel, J.W. Eastwood, Quiet high-resolution computer models of a plasma, J. Comput. Phys. 14 (2) (1974) 148–158.

[46] S. Nosé, A molecular dynamics method for simulations in the canonical ensemble, Mol. Phys. 52 (2) (1984) 255–268.

[47] W.G. Hoover, Canonical dynamics: Equilibrium phase-space distributions, Phys. Rev. A 31 (1985) 1695.

[48] S. Nose, M.L. Klein, Constant pressure molecular dynamics for molecular systems, Mol. Phys. 50 (1983) 1055–1076.

[49] M. Parinello, A. Rahman, Polymorphic transitions in single crystals: A new molecular dynamics method, J. Appl. Phys. 52 (1998) 7182.

[50] P. Virtanen, R. Gommers, T.E. Oliphant, M. Haberland, T. Reddy, D. Cournapeau, E. Burovski, P. Peterson, W. Weckesser, J. Bright, S.J. van der Walt, M. Brett, J. Wilson, K. Jarrod Millman, N. Mayorov, A.R.J. Nelson, E. Jones, R. Kern, E. Larson, C. Carey, I. Polat, Y. Feng, E.W. Moore, J. VanderPlas, D. Laxalde, J. Perktold, R. Cimrman, I. Henriksen, E.A. Quintero, C.R. Harris, A.M. Archibald, A.H. Ribeiro, F. Pedregosa, P. van Mulbregt, S... Contributors, SciPy 1.0: Fundamental algorithms for scientific computing in Python, Nature Methods 17 (2020) 261–272.

[51] N. Michaud-Agrawal, E.J. Denning, T.B. Woolf, O. Beckstein, MDAnalysis: A toolkit for the analysis of molecular dynamics simulations, J. Comput. Chem. 32 (10) (2011) 2319–2327.

[52] R.J. Gowers, M. Linke, J. Barnoud, T.J.E. Reddy, M.N. Melo, S.L. Seyler, D.L. Dotson, J. Domanski, S. Buchoux, I.M. Kenney, O. Beckstein, MDAnalysis: A Python package for the rapid analysis of molecular dynamics simulations, in: Proceedings of the 15th Python in Science Conference, 2016, pp. 98–105.

[53] T.E. de Oliveira, F. Leonforte, L. Nicolas-Morgantini, A.-L. Fameau, B. Querleux, F. Thalmann, C.M. Marques, Fluid bilayer phase in aqueous mixtures of fatty alcohol and cationic surfactant, Phys. Rev. Res. 2 (2020) 013075, http://dx.doi.org/10.1103/PhysRevResearch.2.013075.

[54] B.A. Cunningham, A.-D. Brown, D.H. Wolfe, W.P. Williams, A. Brain, Ripple phase formation in phosphatidylcholine: Effect of acyl chain relative length, position, and unsaturation, Phys. Rev. E 58 (3662) (1998).

[55] A.H. de Vries, S. Yefimov, A.E. Mark, S.J. Marrink, Molecular structure of the lecithin ripple phase, Proc. Natl. Acad. Sci. USA 102 (15) (2005) 5392–5396.

[56] J. Katsaras, S. Tristram-Nagle, Y. Liu, R.L. Headrick, E. Fontes, P.C. Mason, J.F. Nagle, Clarification of the ripple phase of lecithin bilayers using fully hydrated, aligned samples, Phys. Rev. E 61 (5668) (2000).

[57] A.I. Boyanov, B.G. Tenchov, R.D. Koynova, K.S. Koumanov, Absence of sub-transition in racemic dipalmitoylphosphatidylcholine vesicles, Biomembranes 732 (1983) 711–713.

[58] K.K. Eklund, J.A. Virtanen, P.K.J. Kinnunen, Involvement of phospholipid stereoconfiguration in the pre-transition of dimyristoylphosphatidylcholine, Biomembranes 793 (1984) 310–312.

[59] J.A.N. Zasadzinski, Effect of stereoconfiguration on ripple phases ($P_{\beta'}$) of dipalmitoylphosphatidylcholine, Biomembranes 946 (1988) 235–243.

[60] S. Hanashima, Y. Yano, M. Murata, Enantiomers of phospholipids and cholesterol: A key to decipher lipid-lipid interplay in membrane, Chirality 32 (3) (2020) 282–298, http://dx.doi.org/10.1002/chir.23171.

[61] C.-M. Chen, T.C. Lubensky, F.C. MacKintosh, Phase transitions and modulated phases in lipid bilayers, Phys. Rev. E 51 (1) (1995) 504–513, http://dx.doi.org/10.1103/physreve.51.504.